MESHLESS METHOD FOR HYDRAULIC JUMP PROBLEM

Syamsuri [1]* and Suheni [2]
[1] Department of Mechanical Engineering, National Taiwan University of Science and Technology,Taiwan
[2] Department of Mechanical Engineering, Adhi Tama Institut of Technology, Surabaya
*email: syam_sby2003@yahoo.com

ABSTRACT

A hydraulic jump is a common phenomenon which can be observed in open channels flow such as rivers and spillways. It can cause damage of the downstream bed and bank of the channel due to process of continuous erosion and degradation. In order to reduce the hydraulic jump destruction, the energy in the hydraulic jump must be dissipated as much as possible. One of methods to improve dissipation of energy is using a corrugated bed. In order to know the effect of a corrugated bed on the hydraulic jump, a Smoothed Particle Hydrodynamic (SPH) model is applied to investigate the characteristic of hydraulic jumps in various corrugated beds. A variety of corrugated beds which are smooth, triangular, trapezoidal, and sinusoidal are considered. The opening of a gate is changed to adjust the hydraulic jump. The conjugate depth ratio, the jump length, the bottom shear stress distribution, and the energy dissipation are reported. The results of the present study are in a good agreement with previous studies. It is found that the sinusoidal bed can dissipate more energy than other beds. As a result, corrugated beds can be used to enhance energy dissipation of hydraulic jump in the open channel.

Keywords: Smoothed particle hydrodynamic, free surface flow, hydraulic jump, corrugated bed.

1 INTRODUCTION

A hydraulic jump in a horizontal channel with a smooth bed has been studied extensively by many researchers [1, 2]. Recently, a number of studies regarding hydraulic jumps have been carried out on rough and corrugated beds. However, the main concern with hydraulic jumps on rough and corrugated beds is that the roughness elements and crest of corrugations might be subjected to cavitation and erosion. Therefore, cavitation and erosion may damage the structure itself. If the crests of corrugations are placed at the upwind side carrying the supercritical flow, the corrugations will not protrude into the flow and then prevent cavitation in the basin [3]. Furthermore, in culvert with corrugated bed, Reynolds shear stress is produced so that the velocity magnitude above the corrugations is reduced.

A hydraulic jump using a numerical model has been investigated by applying the Boussinesq Equations [4]. The Boussinesq equations used to simulate both the sub and supercritical flows and a hydraulic jump in a rectangular channel with an inclined bed. The numerical study of a hydraulic jump on a smooth bed has also been carried out by using the volume of fluid (VOF) and the turbulence model to predict the surface elevation for the hydraulic jump and horizontal velocity downstream of the jump [5].

On the other hand, instead of the mesh-based viewpoint of the simulation domain, meshless methods adopt a particle view throughout the problem domain. One distinct meshless particle method is smoothed particle hydrodynamics (SPH). SPH provides some advantages in comparison with the usual limitations of Eulerian mesh-based methods. SPH conserved mass exactly and has strong capability to deal with free surface and moving interface problems [6]. Thus, it is suitable for modeling dam break flows. Standard SPH is formulated for solving the Navier-Stokes equations [7]. Recently, there have been significant processes in the applications of standard SPH to dam-break behavior modeling. Most of them targeted on 2D coastal flow simulations of fluid-structure interaction [8], wave generation [9], and wave breaking [10]. For practical engineering applications, i.e., hydraulic jump, only few studies have attempted to investigate this topic. SPH provided good average pressures values at the bottom of the basin in the jump influence area, but large dispersion was observed for instantaneous water height values [11]. It was considerably improved by introducing another turbulence model.

Although some investigations have recently been carried out on hydraulic jumps on corrugated bed, the information regarding the effects of corrugation on hydraulic jump characteristics is incomplete. The objective of this research is to investigate the effect of smooth, triangular, trapezoidal, and sinusoidal beds on the characteristics of a jump and classification of

hydraulic jump using SPH method. Also, the shear stress on those beds has been determined and reported.

2 SPH FORMULA FOR INCOMPRESSIBLE FLUID FLOW

2.1. Fundamentals of SPH Method

SPH is an interpolation method which allows a function to be expressed in terms of its values at a group of disordered particles [7]. The fundamental principle is to approximate a function A{r} by:

$$A(r) = \int A(r')w(r - r', h)dx' \quad (1)$$

Where h is called the smoothing length and w(r - r', h) is the weighting function or kernel. The integral interpolant is numerically approximated by summation interpolant [7]:

$$A(r) = \sum_b m_b \frac{A_b}{\rho_b} w_{ab} \quad (2)$$

Where the summation is over all the neighboring particles. P_b and m_b are density and mass of a particle, respectively. $w_{ab} = w(r_a - r_b, h)$ is weighting or kernel function. The contribution of each particle to a property is weighted according to their distance from the particle of interest.

2.2. Governing Equations

Governing equations of viscous fluids, which are momentum and mass conservation equations can be presented in the followings:

$$\frac{Dv}{Dt} = -\frac{1}{\rho}\nabla P + g + V_o \nabla^2 v \quad (3)$$

and

$$\frac{1}{\rho}\frac{Dv}{Dt} + \nabla \cdot v = 0 \quad (4)$$

Where ρ is density, v is velocity vector, P is pressure, g is acceleration due to gravity, and V is kinematic viscosity.

In conventional SPH notation of momentum and mass equations, artificial viscosity Π has been used [12]:

$$\frac{Dv_a}{Dt} = -\sum_b m_b \left(\frac{P_b}{{\rho_b}^2} + \frac{P_a}{{\rho_a}^2} + \Pi\right)\nabla_a w_{ab} + g \quad (5)$$

$$\frac{D\rho_a}{Dt} = -\sum_b m_b v_{ab} \nabla_a w_{ab} \quad (6)$$

In the above equations, $\nabla_a w_{ab}$ is the gradient of the kernel with respect to the position of particle a. P_k and ρ_k are pressure and density of particle k (evaluated at a or b)

$$\Pi = \begin{pmatrix} \frac{-\alpha \bar{c}_{ab}\, \mu_{ab}}{\bar{\rho}_{ab}} & v_{ab}\, r_{ab} < 0 \\ 0 & v_{ab}\, r_{ab} > 0 \end{pmatrix} \quad (7)$$

From where α is an empirical coefficient, $\bar{c}_{ab} = (c_a + c_b)/2$, $\bar{\rho}_{ab} = (\rho_a + \rho_b)/2$ and $\mu_{ab} = \frac{h v_{ab} r_{ab}}{{r_{ab}}^2 + 0.01h^2}$ with $v_{ab} = v_a - v_b$ and $r_{ab} = r_a - r_b$ being r_k and v_k the position and velocity corresponding to particle k (a or b). The parameter α must be suitably chosen for a stable and accurate solution. Usually this parameter is $O(10^{-2})$ for free surface flows [13]. Large value of α would delay the wave breaking phenomena [14].

In general, the accuracy of the SPH interpolation increases with the order of the polynomial used in the weighting function [15]. The quintic kernel can constitute a good choice since it provides a higher order of interpolation.

The quintic kernel function from multifarious possible kernel is used in this work,

$$w_{ab} = w(r_a - r_b, h) = \alpha_N \left(1 - \frac{q}{2}\right)^4 (2q + 1), \quad 0 \le q \le 2 \quad (8)$$

Where $q = r_{ij}/h$ and $\alpha_N = 7/(4\pi h^2)$ for 2-D, $\alpha_N = 21/(16\pi h^3)$ for 3-D, $r_{ij} = |r_i - r_j|$ and the coefficient h is the smoothing length.

The tensile correction is automatically activated when using kernels with first derivatives that go to zero with decreasing inter-particle spacing. The above equations are solved numerically by time stepping. In this work, currently use the modified Beeman algorithm which is found to produce the most stable computation. It is found that using the modified Beeman algorithm combined with the quintic kernel gives the best result.

In addition, particles are moved by the following equation:

$$\frac{dr_a}{dt} = v_a + \epsilon \sum_b m_b \left(\frac{v_a - v_b}{\rho_a}\right) w_{ab} \quad (9)$$

the last term including the parameter $\epsilon \approx 0.5$ is the so-called XSPH correction [7] and ensures that neighboring particles move at approximately the same velocity. It prevents that particles with different velocities occupy neraly the same location.

2.3. Equation of State

The equation of state allows to avoid an expensive computation of the Poisson's equation for pressure. This equation is also modified to give a slower speed of sound, it is suitable for the simulation of the bulk flow of fluid. The equation of state relates the pressure in the fluid to the local density and is denoted as

$$P = B\left[\left(\frac{\rho}{\rho_o}\right)^{\gamma} - 1\right] \quad (10)$$

Herein, $\gamma = 7$, $B = {c_o}^2\rho_o/\gamma$ and c_o is the speed of sound at the reference density ($\rho_o = 1000\,kg/m^3$). Using a value corresponding to the real value of the speed of sound in water, a very small time step must be chosen for numerical modeling in terms of on the Courant-Fredrich-Levy condition. However, the speed of sound should be about ten times faster that the maximum fluid velocity in order to keep the change in fluid density less than 1%.

2.4. Viscosity

Artificial viscosity which originally was used in the equation of motion has a few advantages and disadvantages. First of all, in free surface problems, it plays the role of stabilizer in a numerical scheme. Second, artificial viscosity prevents the particle from interpenetrating [12]. Then, it preserves both linear and angular momentum and has an acceptable manner in the case of rigid body rotations [7]. In contrast, the artificial viscosity has some disadvantages. It is a scalar viscosity which cannot take the flow directionally into account [16], and it causes strong dissipation and affects shear stress in the fluid [12]. Thus, researchers prefer to simulate viscosity in a realistic manner.

One realistic expression of viscosity is the laminar viscosity [17] and Sub-Particle Scale (SPS) technique to model turbulence. SPS approach used to model turbulence in some kinds of particle methods such as MPS [18] and Incompressible SPH [19]. Recently, this expression of viscosity is implemented in the compressible SPH method [12]. Laminar Viscosity and Sub-Particle Scale (SPS) Turbulence is adopted in this study. Implementing SPS approach in diffusion term of momentum equation (Equation 3) gives:

$$\frac{Dv}{Dt} = -\frac{1}{\rho}\nabla P + g + V_o\nabla^2 v + \frac{1}{\rho}\nabla\tau \quad (11)$$

Where $V_o(\nabla^2 v)$ represents the laminar viscosity term, and τ represents SPS stress tensor which is modeled by the eddy viscosity assumption [12]. Momentum equation (Equation 11) described in SPH notation using laminar viscosity and SPS:

$$\begin{aligned}\frac{Dv_a}{Dt} = &-\sum_b m_b\left(\frac{P_b}{{\rho_b}^2} + \frac{P_a}{{\rho_a}^2}\right)\nabla_a w_{ab} + g \\ &+ \sum_b m_b\left(\frac{4V_o v_{ab} r_{ab}}{|{r_{ab}}^2|(\rho_a + \rho_b)}\right)\nabla_a w_{ab} \\ &+ \textstyle\sum_b m_b\left(\frac{\tau_b}{{\rho_b}^2} + \frac{\tau_a}{{\rho_a}^2}\right)\nabla_a w_{ab}\end{aligned} \quad (12)$$

Where V_o is the kinetic viscosity of laminar flow (10^{-6} m^2/s).

2.5. Density Reinitialization

While the dynamics predicted by SPH simulations is generally realistic, the pressure field of the particles exhibits large oscillations. Efforts to overcome this problem have been concentrated on several approaches including correcting the kernel [20] and developing an incompressible flow solver. One of the most straight forward and computationally least expensive is to perform a filter over the density of the particles and then re-assign a density to each particle [21]. There are two methods of correction, zeroth order and first order.

The Moving Least Squares (MLS) approach was developed [22] and successfully applied [21, 23]. This is a first-order correction so that the variation of a linear density field can be exactly reproduced by

$$\bar{\rho}_a = \textstyle\sum_b \rho_b {w_{ab}}^{MLS}\frac{m_b}{\rho_b} = \sum_b m_b {w_{ab}}^{MLS} \quad (13)$$

The corrected kernel is evaluated as the following

$${w_{ab}}^{MLS} = {w_b}^{MLS}(r_a) = \beta(r_a)\cdot(r_a - r_b)w_{ab} \quad (14)$$

So that in 2-D

$${w_{ab}}^{MLS} = \begin{bmatrix}\beta_0(r_a) + \beta_{1x}(r_a)(x_a - x_b) \\ +\beta_{1z}(r_a)(z_a - z_b)\end{bmatrix} w_{ab} \quad (15)$$

Where the correction vector β is given by

$$\beta(r_a) = \begin{pmatrix}\beta_0 \\ \beta_{1x} \\ \beta_{1z}\end{pmatrix} = A^{-1}\begin{pmatrix}1 \\ 0 \\ 0\end{pmatrix} \quad (16)$$

and

$$A = \sum_b w_b(r_a)\bar{A}\frac{m_b}{\rho_b} \quad (17)$$

With the matrix $\bar{A}$ given by

$$\bar{A} = \begin{bmatrix} 1 & (x_a - x_b) & (z_a - z_b) \\ (x_a - x_b) & (x_a - x_b)^2 & (z_a - z_b)(x_a - x_b) \\ (z_a - z_b) & (z_a - z_b)(x_a - x_b) & (z_a - z_b)^2 \end{bmatrix} \quad (18)$$

More regular density distribution can be obtained using a MLS density filter [24], so a MLS density filter is used in this study.

3 NUMERICAL MODEL

A hydraulic jump is a type of shock wave where the flow undergoes a sudden transition from swift, thin (shallow) flow to tranquil, thick (deep) flow. Hydraulic jumps are most familiar in the context of open-channel flows. Hydraulic jumps in open-channel flow are characterized as a drop in Froude number F1 defined as

$$F_1 = \frac{v}{\sqrt{gy}} \quad (19)$$

From supercritical ($F_1 > 1$) to subcritical ($F_1 < 1$) conditions. The result is a piecewise increase in depth y and a step decrease in flow velocity v passing through the jump.

The depth of supercritical flow, y_1, "jumps" up to its subcritical conjugate depth, y_2, and the result of this abrupt change in flow conditions is considerable turbulence and energy loss, E_L. Figure 1 shows a schematic of typical jump characteristics where E_1 is the energy of the upstream flow, E_2 is the energy of the downstream flow, and L_i is the length of the hydraulic jump. A series of small surface rollers are formed in a standing wave like the one shown in Figure 1.

Figure 2 shows the schematic of the model for validation. A water bowl is utilized at the tank in order to decrease its volume, to diminish the number of particles, and to reduce the computational time. For this test, the Froude number of the flow upstream of the jump is around 3.5. Monaghan's artificial viscosity is used for validation in the simulation ($\alpha = 0.01$ and $\beta_0 = 0.00$). However, the SPS turbulence model for viscosity is applied for classification and characteristic of hydraulic jump. Fluid particles are initially placed in a staggered grid with the particle spacing dx = dz = 0.2 m.

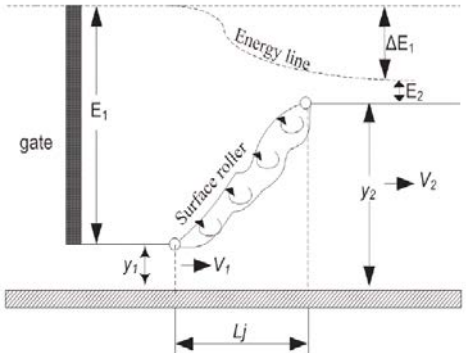

Figure 1. Schematic of hydraulic jump

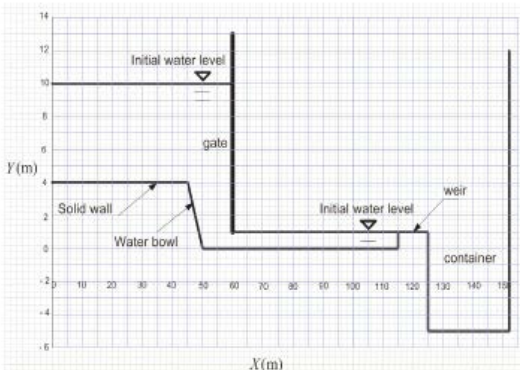

Figure 2. Sketch of tank

3.1. Details of The Basin

The numerical model is conducted and the primary numerical details for different corrugated beds are shown in Figure 3. A hydraulic jump is produced in a rectangular flume which is 1 m deep and 60 m long without a weir crest is installed. Corrugated sinusoidal sheets, corrugated triangular sheets and trapezoidal sheets (see Figure 3) are installed on the flume bed in such a way that the crests of corrugations are at the same level as the upstream bed where the supercritical stream is produced by a sluice gate. The corrugations act as depressions in the bed and create numbers of turbulent eddies which might increase the shear stress on the bed surface. All the three types of corrugations have a wavelength s of 0.19 m in the flow direction and an amplitude t_c of 0.19 m. Where $t_c/y_1 = 0.36$, $s = t_c$, and $\theta = 45°$ are used. t_c/y_1 is defined as the ratio of the amplitude of the corrugation to the initial depth [25]. One of the two trapezoidal sections and the triangular section have the slope of 45°. The discharge is 10.96 m^3/s. Water enters the flume under a sluice gate with a streamlined lip, producing a uniform supercritical stream with a thickness of y_1. A tailgate is used to control the tailwater depth in the flume. In this

study, the tailgate is adjusted so that the jumps are formed on the corrugated beds (see Figure 3).

The initial depth y_1 measured above the crest level of corrugations on the plane bed is equal to 1.76, 1.618, 1.45, 1.252, 1.109, 0.846, 0.788, 0.698, and 0.63 for different Froude numbers. Values of y_1 and V_1 are selected to achieve a wide range of the Froude numbers from 1.5 to 7.0. The Reynolds number $Re = V_1 y_1/\upsilon$ varies from $6.90E^{-06}$–$1.095E^{-07}$.

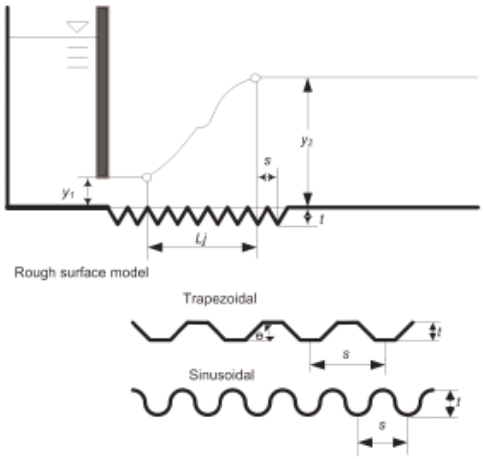

Figure 3. Definition sketch for free jumps on corrugated bed

3.2. Initial Condition and Boundary Conditions

The initial condition is designed to fit the experimental conditions [11]. The present computational system consists of fluid particles and walls. The still water depth is 10 m. The opening of the gate is 1 m. The crested weir is 1 m high. The basin is 115 m long. Froude number in this case is around 3.5. The total number of particles in the numerical model is 22,000 (including 2,723 boundaries particle). Another study uses 11,000 particles to simulate this problem [11].

Solid boundaries are defined by lines of particles that exert repulsive forces on fluid particles [26] in this paper. It is natural to choose central forces similar to those in molecular dynamics [27], but they produce the equivalent of a corrugated boundary with ripples on the scale of the particle spacing.

Boundary particles are distributed evenly (along the boundary) and have a local unit normal vector n that points from the boundary into the fluid. The force per unit mass f on a fluid particle from a boundary particle is computed using the components of their separation along the normal (denoted below by y) and along the tangent (x). The distances x and y are taken as positive. The force then takes the form

$$f = nR(y)P(x) \tag{20}$$

where R(y) is designed to fall to zero within a few particle spacing of the wall and P(x) is designed to ensure that as a fluid particle moves between two boundary particles the contributions from the particles will combine to make the boundary force constant if the fluid particle moves and parallels to the boundary.

Fixed solid particles are allocated in the two rows to form a staggered grid with dx = dz = 0.1 m and zero initial velocity. Their positions remain unchanged during the numerical simulation (V^{solid} (t) = 0 and r^{solid} (t) = r^{solid} (0)).

4 NUMERICAL RESULTS AND DISCUSSION

4.1. Validation of The Model

First, we consider an experimental case previously investigated [11] and shown in Figure 2. 22,000 particles are used in this case. The initial condition [11] is described in Section 3.1. The simulation is performed in a workstation with two 3.40GHz Intel CPU and 3GB RAM. It spends less than 72 hours CPU time to compute results up to the total time of 20 seconds.

Table 1 summarizes the characteristic parameters for a mobile hydraulic jump: the initial depth (y_1), velocity (v_1), Froude number (F_1), location of the jump front (X_{in}), and conjugate depth (y_2). The last three columns in Table 1 compare the analytical conjugate depth is given by the well-known Belanger's equation

$$y_2 = \frac{y_1}{2}\sqrt{1 + 8F_1^{\,2}} - 1 \tag{21}$$

The reason for this discrepancy between analytic and numerical solutions may be the inviscid or friction less flow assumption which means that viscous effect and sidewall friction in Equation 21 is ignored along the bed in the analytic solution.

Tabel 1. Results for validation

Time (s)	y_1 (m)	v_1 (m/s)	F_1	y_2 (analytic) (m)	y_2 (SPH1) (m)	y_2 (SPH2) (m)
5	0.84	10.30	3.59	3.87	3.08	3.10
10	0.80	10.05	3.58	3.68	3.52	3.53
15	0.80	10.03	3.6	3.71	3.70	3.72
20	0.78	9.29	3.36	3.34	3.35	3.38

Notes:
SPH1 is using artificial viscosity
SPH2 is using SPS turbules model for viscosity

Figure 4 shows the comparison between numerical and experimental free surface profiles [11] at successive time steps. While the gate is open, fluid particles flow into the basin. This flow gives rise to a mobile hydraulic jump that travels downstream. The water level at point A is lower than the depth of the jump at point B.

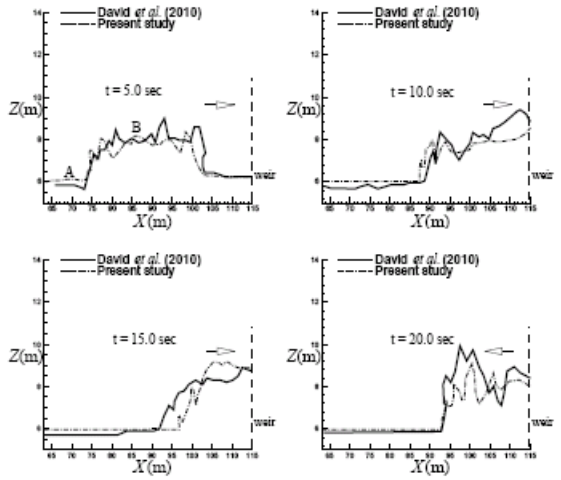

Figure 4. The comparison of surface profiles of hydraulic jump at t 5.0, 10.0, 15.0, 20.0 seconds

It happens at 5 seconds after the gate is opened. This surface profile looks like a "crown" shape. After 10 seconds, the wave arrives in front of the weir and generates a critical section that imposes a higher free surface level of the jump. A wave of higher elevation is evident in the area surrounding the weir. Afterwards, this wave propagates to the downstream direction and then hydraulic jump remain constant. This happens at t = 15 seconds. The hydraulic jump reflected by the weir returns upstream arrives the front of the jump at t = 20 seconds. The lower flow velocity caused by the decrease in reservoir level forces the jump to return upstream. The numerical prediction is in satisfactory agreement with the experimental results.

4.2. Classification of Hydraulic Jump

Hydraulic jumps can be classified according to Froude number or the energy dissipation efficiency. In this present study, only four types of jump are discussed because the surface profile of a hydraulic jump does not exist in a real jump if Froude number >5.0 [11]. In this current study, the classification of this jump is based on the conjugate depth ratio y_2/y_1 [28, 29]. Figure 5 shows free surface profiles and vorticity contours at successive time instants. For $F_1 \leq 1.0$, the flow is critical and hence no jump can form as shown in Figure 5(a). For F_1 = 1 to 1.7, the water surface shows undulations and the jump is called an undular jump as presented in Figure 5(b). In Figure 5(c), a series of small rollers develop below the surface of the jump, but the downstream water surface remains smooth for F_1 = 1.7 to 2.5. This may be called a weak jump. There is an unstable jump. In the beginning, high velocity of flow enters the jump. Afterwards this flow oscillates from the bed to surface and back for F_1 = 2.5 to 4.5. Each oscillation produces a large wave, which can travel and damage structure. This jump may be called an oscillating jump (Figure 5(d)). The classification of the smooth bed has in agreement with previous studies [28, 29].

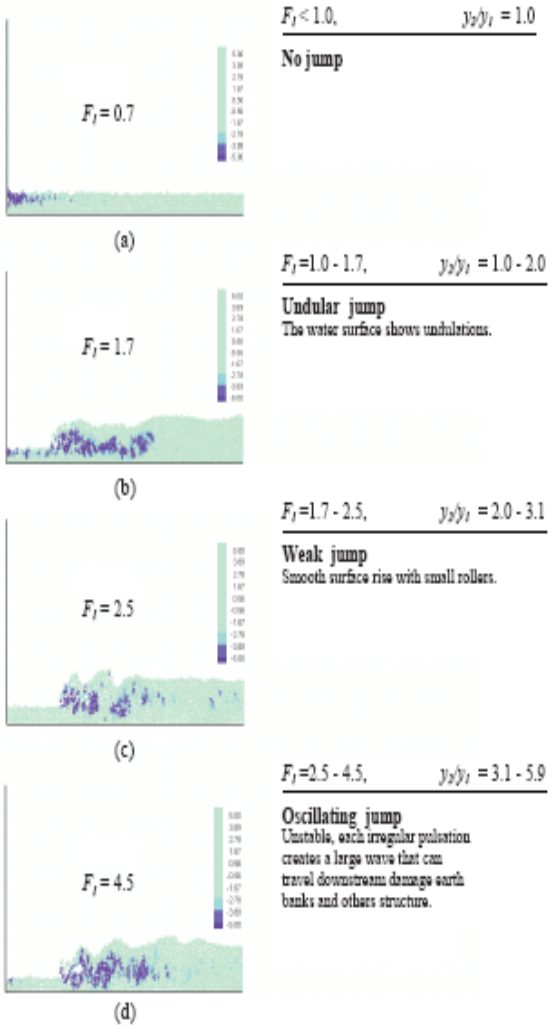

Figure 5. The water surface profiles and vorticity contours of hydraulic jump for F_1 (a) 0.7 (b) 1.7 (c) 2.5 (d) 4.5

Figure 6 shows the relationship between conjugate depth ratio y_2/y_1 and F_1 with different

corrugated beds. In general, for all cases, as F_1 increases (moves toward more supercritical flow), the conjugate depth ratio also increases. The corrugation of the basin also affects the conjugate depth ratio as shown in Figure 6. For the supercritical flow in a horizontal rectangular channel, the energy of flow is dissipated through frictional resistance along the channel and therefore velocity of flow decreases. The conjugate depth also decreases. The main reason of this effect is the increase of the shear stress due to the corrugation of the bed. The results have a reasonable agreement with the experimental study proposed by [25] and with the numerical study by [30].

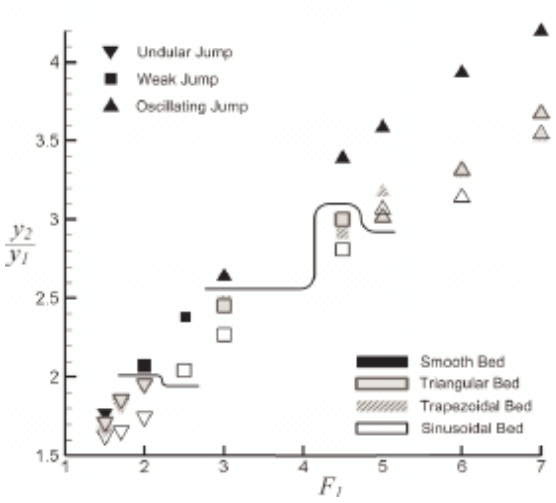

Figure 6. The classification of hydraulic jump for different corrugated bed

Generally, the conjugate depth ratio of corrugated bed especially sinusoidal bed is reduced much in comparison with the smooth bed. As an example for F_1 less than and equal to 1.5, the reduction of conjugate depth ratio is about 8.0%. On the other hand, given that F_1 is more than and equal to 7.0, the reduction will be about 16.0%.

In addition to this, the classification of hydraulic jump change as the bed corrugated change as seen in Figure 6. For an instance, if F_1 is equal to 2.0, the characteristics of the hydraulic jump of the smooth bed will be a weak jump. On the other hand, for triangular, trapezoidal, and the sinusoidal beds, there will be an undular jump. And also for F_1 equal to 3.0, the characteristic of the hydraulic jump of the smooth bed is an oscillating jump. There will be a weak jump for other corrugations. The existence of corrugations not only reduces the length of jump ratio and conjugate depth ratio but also changes the characteristic of hydraulic jump.

4.3. Characteristic of Hydraulic Jump

4.3.1 The bottom shear stress

The shear stress can be estimated by The Sub Particle Scale (SPS) approach to model turbulence [18]

$$\frac{\tau_{ij}}{\rho} = 2\nu_t S_{ij} - \frac{2}{3}k\delta_{ij} - \frac{2}{3}C_1\Delta^2\delta_{ij}\left|S_{ij}\right|^2 \quad (22)$$

where τ_{ij} is the sub-particle stress tensor, ν_t is the turbulence eddy viscosity $[(C_s\Delta 1)]^2|S|$, k is the SPS turbulence kinetic energy, C_s is the Smagorinsky constant (0.12), C_I is 0.0066, $\Delta 1$ is the particle-particle spacing, $|S| = \left(2S_{ij}\,S_{ij}\right)^{1/2}$, and S_{ij} is the element of SPS strain tensor.

The variation of the shear stress with the Froude number is shown in Figure 7. The shear stress profiles for jumps on various corrugated beds are obtained by Equation 22 and compared with the smooth bed case. Solid lines in Figure 7 depict the second order polynomial curve fitting of points, which is the best fitting in this case. It is found that the bottom shear stress downstream of hydraulic jump is smaller than that upstream. It is also found that the bottom shear stress decreases continuously with the distance from toe of the jump and then reaches a constant towards the end of the jump. This is due to the interaction between the supercritical stream with corrugations.

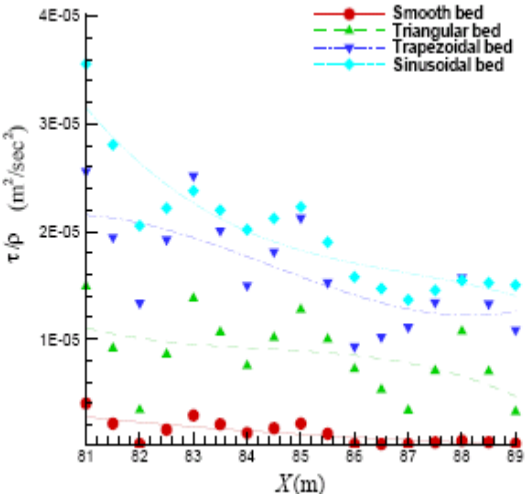

Figure 7. Comparison of bottom shear stress for different corrugated bed, using polynomial second order

The shear stress of sinusoidal bed cases is higher than the smooth bed case. For example, at x = 81 m and 89 m the bottom shear stress $\left(\tau_{ij}\backslash\rho\right)$ in the z-direction is 3.6E^{-05} and 1.6E^{-05}, this value is

higher than that in the smooth bed case. The results have a suitable agreement with the others experimental study [3, 25, 31] and with the numerical study [30].

The maximum of shear stress occurs in the sinusoidal bed case. Trapezoidal bed and triangular bed cases are the second and the third, respectively. This order can be seen again for the other corresponding parameter of hydraulic jump like corrugate depth ratio.

5 CONCLUSSIONS

In the present study, a SPH model has been established to simulate characteristics of hydraulic jump in a corrugated bed. Four various models including a smooth bed, a triangular bed, a trapezoidal bed, and sinusoidal bed are considered to study the effect of corrugation on hydraulic jump. Variations of hydraulic jump due to different corrugations have been predicted by the proposed SPH model successfully. The shear stress at the bottom is determined along the flow direction. A corrugated bed induces more shear stress than a smooth bed. The highest shear stress distribution occurs in the sinusoidal bed case. This finding agrees with previous experimental studies [3, 25, 31] and the numerical study [30]. The energy dissipation in hydraulic jump is calculated as well. In terms of numerical results, it turns out that a corrugated bed can dissipate more energy in hydraulic jump than a smooth bed. Among those three corrugated beds, the sinusoidal bed has the highest energy dissipation in hydraulic jump.

The results of the present study show that corrugated beds can be effectively decrease the conjugate depth ratio and the length of jump ratio. Among those three corrugated beds, the sinusoidal bed can reduce the hydraulic jump mostly and causes more energy dissipation. In conclusion, this study may provide useful information and a useful tool for an engineer who would like to design a corrugated bed to avoid the damage of hydraulic jump in a channel.

REFERENCES

[1] Vischer D L and Hager W H (1995) Energy dissipators, IAHR hydraulic structures design manual. Rotterdam: Balkema.

[2] Saman N and Ali T (1995) Hydraulic jumps on adverse slope in two case of rough and smooth bed. Research Journal of Applied Sciences, Engineering, and Technology 2(2): 19-22.

[3] Ead S A, Rajaratnam N, Katopodis C, and Ade F (2000) Turbulent open-channel flow in circular corrugated culverts. Journal of Hydraulic Engineering 126: 750-757.

[4] Gharangik A M and Chaundhry M H (1991) Numerical model of hydraulic jump. Journal of Hydraulic Engineering 117: 1195-1209.

[5] Zhao Q and Misra S K (2004) Numerical study of a turbulent hydraulic jump. Proceeding of 17th Engineering Mechanics Conference. University of Delaware, Newark, Delaware, June 13-16, 2004.

[6] Liu G R and Liu M B (2003) Smoothed particle hydrodynamics: a meshfree particle method. Singapore: World Scientific Publishing.

[7] Monaghan J J (1992) Smoothed particle hydrodynamics. Annual Reviews Astronomy and Astrophysics 30(1): 543-574.

[8] Crespo A J C, Gesteira G M, and Dalrymple R A (2010) SPHysics-FUNWAVE hybrid model for coastal wave propagation. Journal of Hydraulic Research 48: 85-93.

[9] Yim S C, Yuk D, Panizzo A, Di Risio M, and Liu P L F (2008) Numerical simulations of wave generation by a vertical plunger using RANS and SPH models. Journal of Waterway, Port, Coastal, and Ocean Engineering 134(3): 143-159.

[10] Shao S (2006) Incompressible SPH simulation of wave breaking and overtopping with turbulence modeling. International Journal for Numerical Methods in Fluids 50(5): 597-621.

[11] David L, Roberto M, and Luis G (2010) Smoothed particle hydrodynamics model applied to hydraulic structure: a hydraulic jump test case. Journal of Hydraulic Research 48(1): 142-158.

[12] Dalrymple R A and Rogers B D (2006) Numerical modeling of water waves with the SPH method. Coastal Engineering 53(2): 141-147.

[13] Colagrossi A (2005) A meshless lagrangian method for freesurface and interface flows with fragmentation. PhD Thesis, University of Rome, Italy.

[14] Delorme L, Colagrossi A, Souto-Iglesias A, Zamora-Rodrýguez R, and Botia-Vera E (2009) A set of canonical problems in sloshing, part I: pressure field in forced roll-comparison between experimental results and SPH. Ocean Engineering 36(2): 168-178.

[15] Capone T, Panizzo A, Cecioni C, and Dalrymple R A (2007) Accuracy and stability of numerical schemes in SPH.

Proceedings of SPHERIC Second International Workshop. Madrid, Spain, May 23-25, 2007.

[16] Khayyer A and Gotoh H (2008) Development of CMPS method for accurate water-surface tracking in breaking waves. Coastal Engineering 50(2): 179-207.

[17] Morris J P, Fox P J, and Zhu Y (1997) Modeling lower reynolds number incompressible flows using SPH. Journal of Computational Physics 136 (1): 214-226.

[18] Gotoh H, Shibihara T, and Sakai T (2001) Sub-particle-scale turbulent model for the MPS method-Lagrangian flow model for hydraulic engineering. Advanced Methods for Computational Fluid Dynamics 9(4):339-347.

[19] Shao S D and Lo E Y M (2003) Incompressible SPH method for simulating newtonian and non-newtonian flows with a free surface. Advances in Water Resources 26(7): 787-800.

[20] Bonet J and Lok T S (1999) Variational and momentum preservation aspects of smooth particle hydrodynamic formulations. Computer Methods in Applied Mechanics and Engineering 180 (1): 97-115.

[21] Colagrossi A and Landrini M (2003) Numerical simulation of interfacial flows by smoothed particle hydrodynamics. Journal of Computational Physics 191(2): 448-475.

[22] Dilts G A (1999) Moving-least-squares-particle hydrodynamics-I. Consistency and stability. International Journal for Numerical Methods in Engineering 44(8): 1115-1155.

[23] Panizzo A (2004) Physical and numerical modelling of sub-aerial landslide generated waves. PhD Thesis, Universita degli studi di L'Aquila, L'Aquila, Italy.

[24] Crespo A J C, Gomez-Gesteira M, and Dalrymple R A (2007) Boundary conditions generated by dynamic particles in SPH methods. CMC: Computers, Materials, and Continua 5(3): 173-184.

[25] Ibrahim H E and Shazy S (2010) Formation of hydraulic jumps on corrugated bed. International Journal of Civil and Environmental Engineering 10(1): 40-54.

[26] Peskin C S (1977) Numerical analysis of blood flow in the heart. Journal of Computational Physics 25(3): 220-252.

[27] Monaghan J J and Kos A (1999) Solitary waves on a cretan beach. Journal of Waterway, Port, Coastal, and Ocean Engineering 125(3): 145-154.

[28] Bureau of Reclamation US (1955) Research studies on stilling basins, energy dissipators, andassociated appurtenances. Hydraulic Laboratory Report No. Hyd-399.

[29] Munson B R, Young D F, and Okiishi T H (2002) Fundamental of fluid mechanics. US: John Wiley & Sons Inc.

[30] Abbaspour A, Farsadizadeh D, Dalir A H, and Sadraddini A A (2009) Numerical study of hydraulic jumps on corrugated beds using turbulence models. Turkish Journal of Engineering Environmental Science 33(1): 61-72.

[31] Farhad I and Mahmood S B (2007) Corrugated beds hydraulic jump stilling basin. Journal of Applied Sciences 7(8): 1164-1169.